

Tunable nonlinear \mathcal{PT} -symmetric defect modes with an atomic cell

Chao Hang¹, Dmitry A. Zezyulin², Vladimir V. Konotop², and Guoxiang Huang¹

¹State Key Laboratory of Precision Spectroscopy and Department of Physics, East China Normal University, Shanghai 200062, China

²Centro de Física Teórica e Computacional and Departamento de Física, Faculdade de Ciências, Universidade de Lisboa, Instituto para Investigação Interdisciplinar, Avenida Professor Gama Pinto 2, Lisboa 1649-003, Portugal

Compiled June 29, 2021

We propose a scheme of creating a tunable highly nonlinear defect in a one-dimensional photonic crystal. The defect consists of an atomic cell filled in with two isotopes of three-level atoms. The probe-field refractive index of the defect can be made parity-time (\mathcal{PT}) symmetric, which is achieved by proper combination of a control field and of Stark shifts induced by a far-off-resonance field. In the \mathcal{PT} -symmetric system families of stable nonlinear defect modes can be formed by the probe field. © 2021 Optical Society of America

OCIS codes: 190.0190,190.6135,190.3270.

Defects are known to play an important role in controlling, manipulating and guiding light. Depending on the physical nature of a defect, one can distinguish conservative and nonconservative (i.e. active or dissipative) defects, as well as linear and nonlinear ones, which display very different properties with respect to the modes they support. In particular, nonlinear conservative defects embedded in a linear structure can support families of the modes, whose propagation constant depends on the field intensity (representing the so called families of solitons). Meantime, the modes supported by nonconservative (active) defects have been attracting increasing recent attention, see [1, 2] and [3] for a brief review. Shapes and propagation constants of such modes are strictly determined by the system parameters (mathematically, such modes are isolated fixed points).

For applications it is desirable to have defects with tunable parameters. To this end there were suggested to employ the electro-optical effect [4] implemented experimentally using a nematic liquid crystal defect layer [5, 6], to control a liquid crystal cell (defect) by magnetic field [7], or to enhance conservative defect modes through the parametric resonance [8]. Tunable active defects can be implemented by using doping of a desired domain of the guiding medium by active impurities like in the experimental setting of Ref. [9], where a parity-time (\mathcal{PT} -) symmetric [10] defect, i.e. a structure with the refractive index obeying $n(x) = \bar{n}(-x)$ [11], was created (hereafter overbars stand for complex conjugation).

In the present Letter, we suggest a way of implementing a tunable *nonlinear* defect in a photonic crystal. The defect can be transformed from a dissipative to a \mathcal{PT} symmetric simply by changing the external control field. In the \mathcal{PT} -symmetric case it allows for existence of continuous families of localized guided modes. (We emphasize the difference between our statement and the recent studies of defect modes with a localized defect placed in a \mathcal{PT} -symmetric lattice [12, 13]).

Following [14], where an optically active \mathcal{PT} -symmetric atomic system was proposed, we consider a

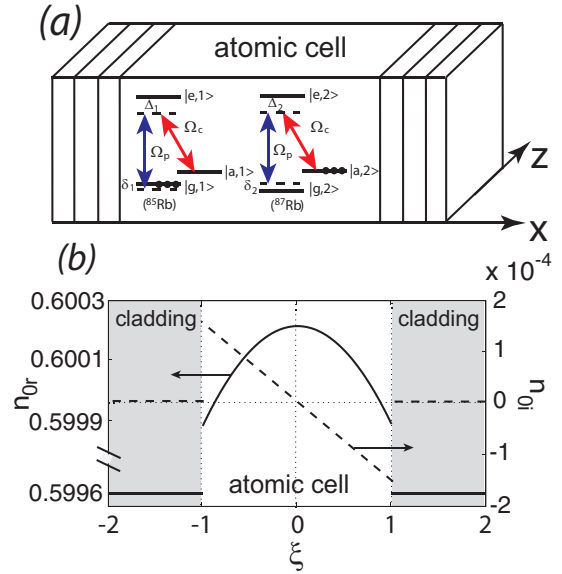


Fig. 1. (Color online) (a) Geometry of the photonic crystal, the energy-level diagram, and Raman resonance scheme of a binary mixture. The initially populated levels are indicated by the black dots. (b) Distribution of real n_{or} (solid line) and imaginary n_{oi} (dashed line) parts of the linear refractive index induced by the fields (4).

cell in a one-dimensional photonic crystal which is filled in by a mixture of two isotopes ($s = 1, 2$) of three-level atoms [Fig. 1(a)]. Like in the original work [15], where the system was introduced for creating large real refractive indexes (see also [16] for comparison with alternative schemes), each isotope is represented by a three-level atom with two ground-state states, $|g, s\rangle$ and $|a, s\rangle$, and one excited state, $|e, s\rangle$.

A weak probe field propagating along z -direction and having the wavenumber k_p and amplitude E_p , induces transitions between the states $|g, s\rangle$ and $|e, s\rangle$ with the Rabi frequency $\Omega_p = p_{eg}E_p/\hbar$, while a strong control field of a wave number k_c and amplitude E_c results

in coupling $|a, s\rangle - |e, s\rangle$ with the Rabi frequency $\Omega_c = p_{ea}E_c/\hbar$. Here p_{eg} and p_{ea} represent the electric dipole matrix elements of the respective inter-level transitions (we assume them to be equal for the both isotopes, i.e. to be independent on s). The one- and two-photon detunings are given respectively by $\Delta_s = \omega_e^s - \omega_a^s - \omega_c$ and $\delta_s = \omega_a^s - \omega_e^s - (\omega_p - \omega_c)$, where ω_l^s ($l = a, e$) is the eigenfrequency of the state $|l, s\rangle$. We also assume that all fields are far-off one-photon resonance but close to the two-photon (i.e. Raman) resonance, i.e. $\Delta_s \gg |\delta_s|$. Each Λ -system is initially prepared in one of the two ground-state states [Fig. 1(a)], such that $s = 1$ and $s = 2$ isotopes with $\delta_1 > 0$ and $\delta_2 < 0$ provide, respectively, the two-photon absorption and gain of the probe field.

Let us highlight some features of the defect created by the proposed atomic cell. First, it uses the same mechanism (i.e. the interaction of the laser field with an atomic cell) to control both gain and dissipation. Second, in resonant atomic media one can create extremely strong nonlinearities [17] (the generation power of the \mathcal{PT} -symmetric defect modes considered below can be reduced to a nanowatt range), thus allowing one to explore nonlinear defects and to operate with nonlinear defect modes embedded in a linear photonic crystal. Third, the shape of the defect can be changed *in situ*. At the same time, it is also relevant that the possibility of direct transfer of the ideas from a linear system (considered in [14]) to a nonlinear one (considered here) is neither evident nor trivial. Indeed, holding the \mathcal{PT} -symmetry with nondissipative (or weakly-dissipative) nonlinearity imposes additional (compared with the linear case) constraints on the parameters of the applied laser beams.

In the paraxial and the weakly guiding approximations the equation governing the envelope of the probe field beam Ω_p reads $2ik_p \frac{\partial \Omega_p}{\partial z} + \frac{\partial^2 \Omega_p}{\partial x^2} + k_p^2 \chi_p \Omega_p = 0$. Here χ_p is the probe-field susceptibility. Outside the atomic cell it equals the effective susceptibility of the Bragg cladding. Inside the cell it is given by $\chi_p = p_{eg}^2 (N_1 \rho_{1g}^s + N_2 \rho_{2g}^s) / (\epsilon_0 \hbar \Omega_p)$, where N_s ($s = 1, 2$) are densities and ρ_{eg}^s are coherences of the s -th atomic specie. The coherences ρ_{eg}^s can be computed from the Bloch equations [19]:

$$i\dot{\rho}_{gg}^s = i\Gamma_{eg}\rho_{ee}^s - \bar{\Omega}_p\rho_{eg}^s + \Omega_p\bar{\rho}_{eg}^s, \quad (1a)$$

$$i\dot{\rho}_{aa}^s = i\Gamma_{ea}\rho_{ee}^s - \bar{\Omega}_c\rho_{ea}^s + \Omega_c\bar{\rho}_{ea}^s, \quad (1b)$$

$$i\dot{\rho}_{ee}^s = -i(\Gamma_{eg} + \Gamma_{ea})\rho_{ee}^s + \bar{\Omega}_p\rho_{eg}^s - \Omega_p\bar{\rho}_{eg}^s + \bar{\Omega}_c\rho_{ea}^s - \Omega_c\bar{\rho}_{ea}^s, \quad (1c)$$

$$i\dot{\rho}_{ag}^s = -d_{ag}^s\rho_{ag}^s + \Omega_p\bar{\rho}_{ea}^s - \bar{\Omega}_c\rho_{eg}^s, \quad (1d)$$

$$i\dot{\rho}_{eg}^s = -d_{eg}^s\rho_{eg}^s + \Omega_p(\rho_{ee}^s - \rho_{gg}^s) - \Omega_c\rho_{ag}^s, \quad (1e)$$

$$i\dot{\rho}_{ea}^s = -d_{ea}^s\rho_{ea}^s + \Omega_c(\rho_{ee}^s - \rho_{aa}^s) - \Omega_p\bar{\rho}_{ag}^s. \quad (1f)$$

In Eqs. (1) the overdots stand for the time derivatives, and we defined: $d_{ag}^s = -\delta_s + i\Gamma_{ag}/2$, $d_{ea}^s = -\Delta_s + i(\Gamma_{eg} + \Gamma_{ea})/2$, and $d_{eg}^s = -\delta_s - \Delta_s + i(\Gamma_{eg} + \Gamma_{ea})/2$ with Γ_{jk} ($j, k = g, a, e$) being the spontaneous emission decay rate from $|j, s\rangle$ to $|k, s\rangle$.

We are interested in the stationary states of (1). Us-

ing the smallness of the intensity of the probe field, i.e. considering $|\Omega_p/\Omega_c| \ll 1$, we look for a stationary solution in the form $\rho_{jk}^s = \sum_{m=0}^{\infty} \rho_{jk,m}^s$ where $j, k = g, a, e$ and $\rho_{jk,m}^s$ is of order of $(\Omega_p/\Omega_c)^m$. Then, in the leading order the system (1) is solved by $\rho_{gg,0}^s = \rho_{aa,0}^s = 1$ and $\rho_{ea,0}^s = -\Omega_c/d_{ea}^s$ with other leading elements of the density matrix being zero. Using the conservation $\rho_{ee,m}^s = \delta_{0,m} - \rho_{gg,m}^s - \rho_{aa,m}^s$ [following from (1a)-(1c)], in higher orders, we obtain the recurrent relations

$$\begin{pmatrix} d_{ag}^s & \bar{\Omega}_c \\ \Omega_c & d_{eg}^s \end{pmatrix} \begin{pmatrix} \rho_{ag,m}^s \\ \rho_{eg,m}^s \end{pmatrix} = \Omega_p \begin{pmatrix} \bar{\rho}_{ea,m-1}^s \\ \rho_{ee,m-1}^s - \rho_{gg,m-1}^s \end{pmatrix}, \quad (2a)$$

$$\begin{pmatrix} i\Gamma_{eg} & i\Gamma_{eg} & 0 & 0 \\ i\Gamma_{ea} & i\Gamma_{ea} & \bar{\Omega}_c & -\Omega_c \\ \Omega_c & 2\Omega_c & d_{ea}^s & 0 \\ -\bar{\Omega}_c & -2\bar{\Omega}_c & 0 & -\bar{d}_{ea}^s \end{pmatrix} \begin{pmatrix} \rho_{gg,m}^s \\ \rho_{aa,m}^s \\ \rho_{ea,m}^s \\ \rho_{ae,m}^s \end{pmatrix} = \mathbf{M}_{m-1}, \quad (2b)$$

where

$$\mathbf{M}_m = \begin{pmatrix} \Omega_p\bar{\rho}_{eg,m}^s - \bar{\Omega}_p\rho_{eg,m}^s & \\ 0 & \\ -\Omega_p\bar{\rho}_{ag,m}^s & \\ \bar{\Omega}_p\rho_{ag,m}^s & \end{pmatrix}.$$

Having computed the coherence ρ_{eg}^s up to the third order of $|\Omega_p/\Omega_c|$, the probe-field susceptibility in the atomic cell can be expressed as $\chi_{p,1} + \chi_{p,3}|\Omega_p|^2$, where the first- and third-order susceptibilities are

$$\chi_{p,1} = \frac{p_{eg}^2}{\epsilon_0 \hbar} (N_1 A_1 + N_2 A_2), \quad (3a)$$

$$\chi_{p,3} = \frac{p_{eg}^2}{\epsilon_0 \hbar \Gamma_{ea}} \sum_{s=1}^2 N_s \frac{d_{ag}^s C_s - B_s}{|\Omega_c|^2 - d_{ag}^s d_{eg}^s}, \quad (3b)$$

with $A_1 = -d_{ag}^1 D_1$, $A_2 = -|\Omega_c|^2 D_2/d_{eg}^2$,

$$B_s = \frac{\Gamma_{ea} d_{ea}^s}{\Gamma_{eg}} \text{Im}(A_s) - |\Omega_c|^2 \text{Im}(D_s),$$

$$C_s = \text{Im} \left(d_{ea}^s D_s - 6 \frac{\Gamma_{ea}}{\Gamma_{eg}} A_s + \frac{|d_{ea}^s|^2}{|\Omega_c|^2} \frac{\Gamma_{ea}}{\Gamma_{eg}} A_s \right),$$

$$D_1 = \frac{1}{d_{ag}^1 d_{eg}^1 - |\Omega_c|^2}, \quad D_2 = \frac{d_{eg}^2}{\bar{d}_{ea}^2 (|\Omega_c|^2 - d_{ag}^2 d_{eg}^2)}.$$

\mathcal{PT} -symmetric spatial distribution of the susceptibility, $\chi_{p,1}(x) = \bar{\chi}_{p,1}(-x)$, is achieved with help of the far-detuned laser field $E_S(x) \cos(\omega_S t)$ [14], referred to as the Stark field. This field induces the shifts of the levels $|j, s\rangle$: $\Delta E_{j,S}(x) = -\alpha_j E_S^2(x)/4$ (here α_j is the scalar polarizability), and as a consequence the x -dependence of the control field $\Omega_c = \Omega_c(x)$. Since within the required accuracy $\alpha_g \approx \alpha_a$, the difference of the Stark shifts between the ground-state sublevels is negligible, i.e. δ_s is not affected by E_S , while $\Delta_s(x) = \Delta_s - (\alpha_e - \alpha_g) E_S^2(x)/4\hbar$, Δ_s being here the one-photon detuning of the s -th isotope in the absence of the Stark field. We notice that the characteristic scale of the $\Delta_s(x)$ modulation is of order of the Stark field wavelength λ_S . For a typical magnitude of the control field $E_c \sim 1$ V/cm ($\Omega_c \sim 10^7$ Hz), the required amplitude of the Stark field is $E_S \sim 10^3$ V/cm.

Being focused into a spot of a millimeter diameter, this requires laser powers of order of 10 W.

As a case example, we explore a mixture of ^{85}Rb ($s = 1$) and ^{87}Rb ($s = 2$) isotopes, and assign $|g, s\rangle = |5S_{1/2}, F = 1\rangle$, $|a, s\rangle = |5S_{1/2}, F = 2\rangle$, and $|e, s\rangle = |5P_{1/2}, F = 1\rangle$. The densities for each isotope are $N_1 \approx 6 \times 10^{14} \text{ cm}^{-3}$ and $N_2 \approx 1.92 \times 10^{15} \text{ cm}^{-3}$. The coherence decay rates are estimated as $\Gamma_{eg} \approx \Gamma_{ea} \approx \pi \times 5.75 \text{ MHz}$ and $\Gamma_{ag} \approx 10^{-3} \Gamma_{eg}$. With sufficiently high accuracy $\alpha_e - \alpha_g = 2\pi\hbar \times 0.1223 \text{ Hz}(\text{cm}/\text{V})^2$ and $p_{eg} = 2.5377 \times 10^{-27} \text{ C cm}$ [18]. The two-photon detunings are chosen as $\delta_1 = -0.18 \Gamma_{eg}$ and $\delta_2 = 1.63 \Gamma_{eg}$. Following the algorithm of [14], we compute that the \mathcal{PT} -symmetric profile of the susceptibility (with parabolic real part and linear imaginary part) can be achieved by using the control and Stark fields with the forms

$$\Omega_c(\xi) = (2.5 + 0.025\xi + 2.4741 \times 10^{-4}\xi^2)\Gamma_{eg}, \quad (4a)$$

$$E_S(\xi) = (1.9394 - 0.2542\xi)E_0, \quad (4b)$$

where $\xi = k_S x$ ($k_S = 2\pi/\lambda_S$) and $E_0 = 5.0 \times 10^3 \text{ V/cm}$.

At this stage it is important to emphasize that Eqs. (4) provide accurate \mathcal{PT} symmetry only for sufficiently small ξ , while for large ξ significant deviations are observed (see the discussion in [14]). This imposes a constraint on the choice of the size of the atomic cell, which is needed to “cut” the undesirable deviations from the \mathcal{PT} symmetry at large ξ . For the sake of definiteness, we impose the size of the cell to be $\lambda_S/\pi \approx 0.04 \text{ mm}$ where $\lambda_S \approx 0.13 \text{ mm}$ is the typical wavelength of the applied Stark field, which in the dimensionless units correspond to the cell occupying the domain $|\xi| < 1$ [Fig. 1(b)].

With the above parameters of the atomic cell and choosing the effective susceptibility for the Bragg cladding $\chi_{\text{clad}} \approx -0.64046$ [20, 21] ($n_{\text{clad}} \approx 0.5996$), the first-order probe-field susceptibility acquires the form

$$\chi_{p,1}(\xi) \approx \begin{cases} \tilde{\chi}_0 + i\tilde{\chi}_1\xi + \tilde{\chi}_2\xi^2, & |\xi| \leq 1, \\ \chi_{\text{clad}}, & |\xi| > 1, \end{cases} \quad (5)$$

where $\tilde{\chi}_0 \approx -0.6398 \approx \chi_{\text{clad}} + 0.0007$, $\tilde{\chi}_1 \approx -3.2380 \times 10^{-4}$, and $\tilde{\chi}_2 \approx -3.6688 \times 10^{-4}$. In Fig. 1(b) we show real and imaginary parts of the linear refractive index of the defect. In order to control the accuracy of \mathcal{PT} symmetry, we calculated the error function [14] $\nu(\xi) \equiv \chi_{p,1}(\xi) - \bar{\chi}_{p,1}(-\xi)$ for $|\xi| \leq 1$. Real and imaginary parts of ν are $\sim 10^{-7}$ and $\sim 10^{-10}$, respectively.

Another important observation is in order here. In an infinite medium the constant part of the refractive index did not play any significant role [14]. In the case of a defect mode, however, it becomes relevant for determining the guiding regime. In particular, it was mentioned above that we are dealing with the weak guidance, which is ensured by the fact that $|\tilde{\chi}_0 - \chi_{\text{clad}}| \sim 10^{-3} \chi_{\text{clad}}$. This gives the order of small parameter $|\Omega_p/\Omega_c|^2 \sim 10^{-3}$ and hence defines the accuracy of the expansion.

Turning to the third-order probe-field susceptibility, we compute it using Eq. (3b). For the above given parameters inside the atomic cell ($|\xi| \leq 1$) we find $\tilde{\chi}_{p,3} \approx$

-0.1294×10^{-14} . Generally speaking, the real and imaginary parts of $\tilde{\chi}_{p,3}$ depend on the spatial coordinates and also violate the \mathcal{PT} symmetry. These effects, however, are 10^{-2} times smaller than the leading order, i.e. are beyond the accepted accuracy. Now, from the relation $n_2 = p_{eg}^2 \tilde{\chi}_{p,3} / (2\hbar^2 n_0)$, we estimate $n_2 \approx -0.6244 \text{ cm}^2 \text{V}^2$ for the defect. This is about 10^{16} larger than that measured for passive optical materials. Such enhancement of the nonlinearity occurs the existence of two nearly resonant Raman transitions.

Resuming the above parameters, the probe field in the cell is described by the nonlinear Schrödinger equation with a \mathcal{PT} -symmetric linear potential, while outside the cell the system is described by the linear equation:

$$i\frac{\partial u}{\partial \zeta} + \frac{\partial^2 u}{\partial \xi^2} - (iV_1\xi + V_2\xi^2)u - |u|^2 u = 0, \quad |\xi| < 1, \quad (6a)$$

$$i\frac{\partial u}{\partial \zeta} + \frac{\partial^2 u}{\partial \xi^2} - V_0 u = 0 \quad |\xi| \geq 1. \quad (6b)$$

Here $u = \Omega_p e^{-ik_p \tilde{\chi}_0 z/2} / \Omega_0$ is the dimensionless field, whose normalization constant Ω_0 is chosen to scale out the nonlinear coefficient in (6a), $\zeta = (k_S^2/2k_p)z$, $V_0 = (k_p^2/k_S^2)(\tilde{\chi}_0 - \chi_{\text{clad}})$, $V_{1,2} = -(k_p^2/k_S^2)\tilde{\chi}_{1,2}$. For the mixture of the rubidium isotopes and $\lambda_S = 0.13 \text{ mm}$ (thus $k_p/k_S \approx 10^2$) we have $\Omega_0 = 2.8 \times 10^5 \text{ s}^{-1}$, $V_0 \approx 7.1$, $V_1 \approx 3.2380$, and $V_2 \approx 3.6688$.

Turning now to the properties of the defect modes, we first notice that nonlinear modes in the parabolic \mathcal{PT} -symmetric potential were described in [22]. Here, however, we are dealing with a cut parabolic profile, which naturally affects properties of the system. Indeed, let us consider the linearized version of system (6). Without the nonlinear term in (6a), the stationary guided modes $u = e^{ib\zeta} w(\xi)$ are determined by the eigenvalue problem $\mathcal{L}w = bw$, where b is the propagation constant and the \mathcal{PT} -symmetric operator \mathcal{L} is defined as $\mathcal{L} = \frac{d^2}{d\xi^2} - V(\xi)$ with $V(\xi) = iV_1\xi + V_2\xi^2$ for $|\xi| < 1$ and $V(\xi) = V_0$ otherwise. For the above parameters, we have found numerically that \mathcal{L} has exactly two isolated eigenvalues $b_0 \approx -2.4$ and $b_1 \approx -5.8$ [see Fig. 2(a)] and the continuous spectrum situated on the real axis. Reality of the spectrum of \mathcal{L} is an evidence of the unbroken \mathcal{PT} symmetry.

The existence of the two bound states is supported by the given positive value of V_0 . Adjusting the parameters, one can change $V(\xi)$ and hence the properties of the defect modes. For example, decrease (increase) of χ_{clad} results in sequential appearance (disappearance) of isolated real eigenvalues b meaning change of the number of guided linear modes. In particular, for $\chi_{\text{clad}} > -0.64$ no linear guided modes exists. Increase of the imaginary part of the potential eventually results in the \mathcal{PT} symmetry breaking (for the chosen parameters, $\tilde{\chi}_1$ must be about doubled for the \mathcal{PT} symmetry breaking to occur).

Passing to the nonlinear case, each eigenvalue (i.e. b_0, b_1 , etc.) gives birth to a family of nonlinear modes, as shown in Fig. 2(a) on the plane (U, b) , where $U =$

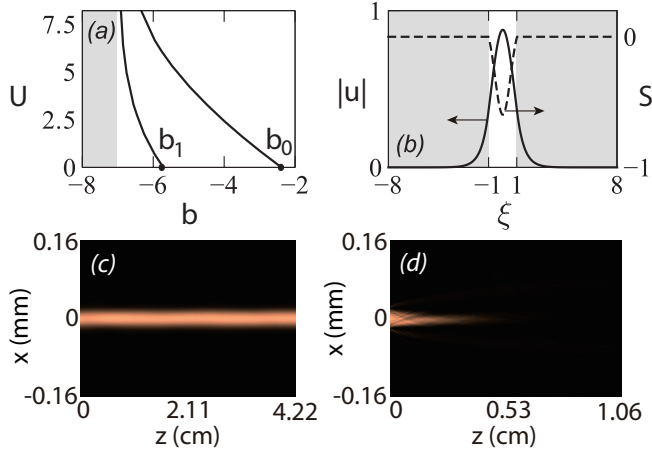


Fig. 2. (Color online) (a): Two families of nonlinear modes bifurcating from the eigenvalues $b_{0,1}$ (see the text). The shaded domain corresponds to propagation constants belonging to the continuous spectrum. (b): The amplitude $|u|$ (solid line) and the current S (dashed line) for the nonlinear mode with $b = -3$. The shaded domain corresponds to the cladding. (c), (d): Evolution of the nonlinear mode intensity $|u|^2$ for the \mathcal{PT} -symmetric (c) and non- \mathcal{PT} -symmetric (d) refractive indexes.

$\int_{-\infty}^{\infty} |u|^2 d\xi$ is the total energy flow. In the linear limit, $U \rightarrow 0$, the propagation constants approach $b_{0,1}$. With the decrease of b the total energy flow monotonously grows. A typical profile of a defect mode is shown in Fig. 2(b), where we also plot the “current” $S = \frac{i}{2}(u \frac{\partial u}{\partial \xi} - \bar{u} \frac{\partial \bar{u}}{\partial \xi})$, which is associated with the power-flow density (i.e. with the Poynting vector) in the transverse direction. This current arises from the nontrivial phase structure of the nonlinear modes. The mode shown in Fig. 2(b) is well localized inside the atomic cell: 94% of its energy is confined in the cell.

To examine stability of the modes in a practical system, we add small (of order of 5%) random perturbations to both amplitude and phase of the stationary solution shown in Fig. 2(b) and evolve it according to Eqs. (6). The mode displays robust evolution shown in Fig. 2(c). For comparison, in Fig. 2(d), we repeat the evolution of the same input beam after decreasing N_2 by 5% without changing other parameters. In this case, the system is not \mathcal{PT} symmetric any more [specifically, now one has $\chi_{p,1} \approx -0.5860 - (3.3933\xi^2 + 3.9006\xi + i4.9495 - i3.2402\xi) \times 10^{-4}$]. As expected, we observe decay of the mode which is absorbed at relatively short distances.

To conclude, we have proposed a scheme of creating strongly nonlinear tunable defects in photonic crystals. Such defects consist of an atomic cell filled in with a mixture of isotopes of lambda atoms subjected to the control and to the Stark fields. By proper adjusting the parameters of the control field the defect can be made \mathcal{PT} -symmetric and in this case it supports families of stable defect modes of the probe field. Due to flexibility, the model allows one to study the effect of nonlinearity

on the bound state number and to design defects with focusing nonlinearities which in their turn may support the quasi-bound states [23]. The generation power of such defect modes can be reduced to the nanowatt range due to resonant enhancement of Kerr nonlinearity.

Acknowledgments The work was supported by NSF-China under Grant Nos. 11174080 and 11105052, by the Program of Introducing Talents of Discipline to Universities under Grant No. B12024, and by the FCT (Portugal) grants PTDC/FIS-OPT/1918/2012 and PEst-OE/FIS/UI0618/2011.

References

1. W. C. K. Mak, B. A. Malomed, and P. L. Chu, Phys. Rev. E **67**, 026608 (2003).
2. D. A. Zezyulin, Y. V. Kartashov, and V. V. Konotop, Opt. Lett. **36**, 1200 (2011).
3. Y. V. Kartashov, V. V. Konotop, V. A. Vysloukh, and D. A. Zezyulin in ”Spontaneous Symmetry Breaking, Self-Trapping, and Josephson Oscillations” Prog. Optic. Sci. and Photonics **1**, 167-200 (2013).
4. Ha, Y. K., Y. C. Yang, J. E. Kim, and H. Y. Park, Appl. Phys. Lett., **79**, 15 (2001).
5. R. Ozaki, T. Matsui, M. Ozaki, and K. Yoshino, Appl. Phys. Lett. **82**, 3593 (2003).
6. R. Ozaki, H. Miyoshi, M. Ozaki and K. Yosjino, Molecular Crystals and Liquid Crystals, **433**, 247-257 (2006).
7. V. Ya. Zyryanov, S. A. Myslivets, V. A. Gunyakov, A. M. Parshin, V. G. Arkhipkin, V. F. Shabanov, and Wei Lee Opt. Express, **18**, 1283 (2010).
8. V. V. Konotop, and V. Kuzmiak, Phys. Rev. B **64**, 125120 (2001).
9. C. E. Rüter, K. G. Makris, R. El-Ganainy, D. N. Christodoulides, M. Segev, and D. Kip, Nature Phys. **6**, 192 (2010).
10. C. M. Bender, Rep. Prog. Phys. **70**, 947 (2007).
11. A. Ruschhaupt, F. Delgado, J. G. Muga, J. Phys. A: Math. Gen. **38**, L171 (2005)
12. S. Hu, X. Ma, D. Lu, Y. Zheng, and W. Hu, Phys. Rev. A **85**, 043826 (2012).
13. H. Wang and J. Wang, Opt. Express **19**, 4030 (2011).
14. C. Hang, G. Huang, and V. V. Konotop, Phys. Rev. Lett. **110**, 083604 (2013).
15. C. O’Brien, P. M. Anisimov, Y. Rostovtsev, and O. Kocharovskaya, Phys. Rev. A **84**, 063835 (2011).
16. Z. J. Simmons, N. A. Proite, J. Miles, D. E. Sikes, and D. D. Yavuz, Phys. Rev. A **85**, 053810 (2012).
17. V. S. Letokhov, “Laser Control of Atoms and Molecules” (Oxford University Press, New York, 2007).
18. D. Steck, ⁸⁵Rb D Line Data, <http://steck.us/alkalidata>.
19. M. Fleischhauer, A. Imamoglu, and J. P. Marangos, Rev. Mod. Phys. **77**, 633 (2005).
20. J. P. Dowling and C. M. Bowden, J. Mod. Opt. **41**, 345 (1994).
21. J. M. Bendickson, J. P. Dowling, and M. Scalora, Phys. Rev. E **53**, 4107 (1996).
22. D. A. Zezyulin and V. V. Konotop, Phys. Rev. A **85**, 043840 (2012).
23. N. Moiseyev, L. D. Carr, B. A. Malomed, and Y. B. Band, J. Phys. B **37**, L193-L200 (2004)